

Effective Electrostatic Interactions in Solutions of Polyelectrolyte Stars with Rigid Rodlike Arms

Hao Wang* and Alan R. Denton†

Department of Physics, North Dakota State University, Fargo, North Dakota, 58105-5566

(Dated: November 21, 2018)

Abstract

In solutions of star-branched polyelectrolytes, electrostatic interactions between charged arms on neighboring stars can compete with intra-star interactions and rotational entropy to induce anisotropy in the orientational distribution of arms. For model stars comprising rigid rodlike arms with evenly spaced charged monomers interacting via an effective screened-Coulomb (Yukawa) potential, we explore the influence of arm orientational anisotropy on effective star-star interactions. Monte Carlo simulation and density-functional theory are used to compute arm orientational distributions and effective pair potentials between weakly charged stars. For comparison, a torque balance analysis is performed to obtain the configuration and energy of the ground state, in which the torque vanishes on each arm of the two-star system. The degree of anisotropy is found to increase with the strength of electrostatic interactions and proximity of the stars. As two stars begin to overlap, the forward arms are pushed back by inter-star arm-arm repulsion, but partially interdigitate due to rotational entropy. At center-center separations approaching complete overlap, the arms relax to an isotropic distribution. For nonoverlapping stars, anisotropy-induced changes in intra- and inter-star arm-arm interactions largely cancel and the effective pair interactions are then well approximated by a simple Yukawa potential, as predicted by linear response theory for a continuum model of isotropic stars [A. R. Denton, *Phys. Rev. E* **67**, 11804 (2003)]. For overlapping stars, the effective pair interactions in the simple rigid-arm-Yukawa model agree closely with simulations of a molecular model that includes flexible arms and explicit counterions [A. Jusufi, C. N. Likos, and H. Löwen, *Phys. Rev. Lett.* **88**, 018301 (2002); *J. Chem. Phys.* **116**, 11011 (2002)].

PACS numbers: 05.20.Jj, 82.70.Dd, 82.45.-h

* Present address: Dept. of Chemistry, Emory University, Atlanta, Georgia 30322

† Author to whom correspondence should be addressed; electronic mail: alan.denton@ndsu.edu

I. INTRODUCTION

Polyelectrolytes (PEs) are polymers that carry ionizable groups¹. In solution, small ions (counterions) dissociate, creating oppositely charged polyions. Common examples of PEs are polyacrylic acid, sulfonated polystyrene, and biopolymers, such as proteins, DNA, and starch. Practical applications in the chemical, microelectronics, and pharmaceutical industries include water filtration membranes, direct-write technologies², DNA-protein binding, and thin films for controlled drug delivery^{3,4}. When dispersed in an aqueous electrolyte, or other polar solvent, PEs interact electrostatically with one another and with charged surfaces. Bare Coulomb interactions are screened by dissociated microions (counterions and salt ions) distributed in and around the polyions. A fundamental understanding of these microscopic interactions is essential for predicting and controlling equilibrium and dynamical properties of bulk PE solutions.

Beyond linear chains, PEs can be readily synthesized with more complex architectures, such as stars, microgels, block-copolymer micelles, and dendrimers. In this paper, we focus on star-branched PEs, comprising linear PE chains (arms) chemically grafted or adsorbed to a common microscopic core. In sharp contrast to colloidal microspheres, whose hard cores are rigid and impermeable to microions, PE polyions have internal degrees of freedom associated with both chain conformations and microion distributions. Such porous macromolecules are characterized by ultra-soft pair interactions⁵. The main issue addressed here is the extent of anisotropy in arm orientations induced by electrostatic interactions between neighboring stars and the implications for effective interactions between stars in solution.

Chain conformations in PE stars have been extensively modeled by scaling theory^{6,7}, self-consistent field theory⁷, Monte Carlo (MC)⁸ and molecular dynamics (MD)^{9,10} simulations. On the experimental side, several studies have analyzed the structure of PE stars and spherical PE brushes in solution. Small-angle neutron scattering^{11,12,13} and dynamic light scattering¹⁴ measurements indicate that the arms of highly ionized stars are almost fully stretched, a finding supported by simulations^{9,10}. Other neutron scattering studies, using isotopically labelled samples^{15,16,17}, have directly probed counterion distributions, indicating a strong coupling between counterions and PE chains. These studies, together with osmotic pressure measurements¹⁸, support conclusions from theoretical and simulation work^{6,9,10,19,20} that a high fraction of counterions remain trapped inside the stars, screening electrostatic

interactions between the arms.

Comparatively few studies have examined interactions between PE stars. Recently, we applied response theory to a continuum model^{20,21}, in which the density of charged monomers is approximated as an isotropic, continuously varying $1/r^2$ distribution, where r is the radial distance from the star center. Assuming linear screening of bare Coulomb interactions by microions, this approach predicts screened-Coulomb (Yukawa) effective interactions between pairs of nonoverlapping stars. In complementary studies, Jusufi, Likos, and Löwen^{9,10} used simulation and variational theory to calculate effective pair interactions between overlapping stars in a molecular model that includes flexible PE chains and explicit counterions.

Motivated by recent simulations^{9,10} and experiments^{11,12,13,14}, we explore here a relatively simple model of PE stars consisting of rigid rodlike arms, lacking bend and twist flexibility, and carrying charged beads that interact via screened-Coulomb pair potentials. The intrinsic rigidity of PE chains is enhanced in star architecture by electrostatic and solvent-mediated excluded-volume repulsions between arms. For example, DNA and some synthetic stiff PE chains can be assembled into stars with relatively inflexible arms^{22,23,24,25}. The rodlike model, while directly relevant to such systems, also represents a reference model for stars with semiflexible arms.

The outline of the remainder of the paper is as follows. Section II first explicitly defines the rigid-arm model of PE stars. Section III then describes three complementary methods for analyzing arm orientational anisotropy and effective pair potentials between stars: Monte Carlo simulation, torque balance analysis, and density-functional theory. Section IV next presents and discusses numerical results for arm orientational distributions and effective pair potentials. Most significantly, the three independent methods yield consistent results for star-star interactions, which closely agree with molecular dynamics simulations of the molecular model. Finally, Sec. V summarizes and concludes.

II. MODEL

We consider star-branched polyelectrolytes, each star comprising f chains (arms) attached to a central core and freely rotating about the core. As depicted in Fig. 1, the arms are modeled as rigid rods of equal length a , each arm carrying N_b charged monomers (beads) evenly spaced at a neighbor separation b along the arm. The microions in our model play two

essential roles: charge renormalization and electrostatic screening. Most of the counterions condense onto or strongly associate with the arms. These bound counterions reduce the bare charge on the arms, significantly lowering the effective charge. The remaining mobile microions, inside and outside of the stars, screen the bare Coulomb electrostatic interactions. Assuming an average effective valence z per bead, the effective valence per star is $Z = fN_b z$. The stars are dispersed in an electrolyte solvent, approximated as a dielectric continuum of spatially uniform dielectric constant ϵ (primitive model of electrolytes).

In this paper, we restrict attention to “weakly” charged stars, defined as stars whose arms can freely rotate relative to one another and are not orientationally localized. As a simple physical criterion, a star is weakly charged if the increase in electrostatic energy upon rotating an arm half-way towards any nearest neighbor does not significantly exceed the typical thermal energy $k_B T$ at temperature T . In stars not satisfying this criterion, electrostatic interactions overwhelm Brownian motion and the arms are orientationally frozen.

To model pair interactions, we focus on two isolated stars whose centers are separated by a fixed displacement \mathbf{R} . Integrating out the microion degrees of freedom^{20,21} and assuming linear microion screening of bare Coulomb interactions, pairs of charged beads interact via an effective screened-Coulomb (Yukawa) potential²⁶. The electrostatic interaction between two arms, one oriented along a unit vector \mathbf{u} in a star centered at the origin, the other oriented along \mathbf{u}' in a star centered at \mathbf{R} , is then approximated by an effective pair potential

$$v_{\text{arm}}(\mathbf{u}, \mathbf{u}'; R) = \frac{z^2 e^2}{\epsilon} \sum_{i=1}^{N_b} \sum_{j=1}^{N_b} \frac{\exp(-\kappa |\mathbf{R} + i b \mathbf{u} - j b \mathbf{u}'|)}{|\mathbf{R} + i b \mathbf{u} - j b \mathbf{u}'|}, \quad (1)$$

where e is the proton charge, the summation goes over all the charged beads of the two arms, and κ is the Debye screening constant (inverse Debye screening length). For a solution with star number density ρ , salt ion pair number density ρ_s , and salt valence z_s , the screening constant is given by $\kappa = \sqrt{4\pi e^2 (z^2 f N_b \rho + 2z_s^2 \rho_s) / (\epsilon k_B T)}$.

The orientational distribution of the arms in two interacting stars is determined by a balance of three competing factors. Repulsive forces between arms on different stars exert torques that rotate the arms back, creating anisotropy in the arm distribution. Opposing this backward rotation, repulsions between arms on the same star exert torques that spread out the arms, favoring isotropy. Likewise, random thermal (Brownian) rotational motion acts to even out the arm distribution. To calculate the equilibrium arm distribution, and

the corresponding star-star interaction energy, we use three independent methods, described in the next section.

III. METHODS

A. Monte Carlo Simulation

For our simple rigid-arm model, Monte Carlo simulation proves to be an efficient method for determining the equilibrium distribution of arm orientations at constant temperature. The orientation of an arm, denoted by unit vector \mathbf{u} , is specified in spherical coordinates by polar and azimuthal angles (θ, ϕ) . As illustrated in Fig. 2, for a randomly chosen arm i , a trial rotation is performed from the old orientation $\mathbf{u}_i^{(o)}$ to a new orientation $\mathbf{u}_i^{(n)}$. Adopting an efficient and reliable algorithm²⁷, we generate a new (trial) orientation according to

$$\mathbf{u}_i^{(n)} = \frac{\mathbf{u}_i^{(o)} + \gamma \mathbf{v}}{|\mathbf{u}_i^{(o)} + \gamma \mathbf{v}|}, \quad (2)$$

where \mathbf{v} is a unit vector with random orientation and γ is a tolerance factor that determines the magnitude of the trial rotation. The standard Metropolis scheme gives the probability of accepting a rotation:

$$\text{acc}(o \rightarrow n) = \min \left\{ 1, \exp \left(-\beta [\Phi_{\text{arm}}(\mathbf{u}_i^{(n)}; R) - \Phi_{\text{arm}}(\mathbf{u}_i^{(o)}; R)] \right) \right\}, \quad (3)$$

where $\beta = 1/k_B T$ and $\Phi_{\text{arm}}(\mathbf{u}_i; R)$ represents the electrostatic energy of the i^{th} arm with orientation \mathbf{u}_i in a star at center-center separation R from a second star. The latter energy can be expressed as a sum over arm-arm interactions:

$$\Phi_{\text{arm}}(\mathbf{u}_i; R) = \sum_{j=1 \neq i}^f v_{\text{arm}}(\mathbf{u}_i, \mathbf{u}_j; 0) + \sum_{j=1}^f v_{\text{arm}}(\mathbf{u}_i, \mathbf{u}_j; R), \quad (4)$$

where the first summation includes arms of the same star, excluding self-interaction, and the second summation includes arms of the second star.

Our simulations are initialized by centering one star at the origin, the other at a distance R away along the z -axis, and assigning random orientations to the arms. Next, trial rotations

of the arms are performed in cycles, a cycle consisting of one attempted rotation of each arm, selected sequentially. Following an initial equilibration stage of typically 10^3 cycles, during which the energy is monitored until it reaches a plateau, arm orientation statistics are accumulated in the following 2×10^5 cycles. The average energy of the two-star system is calculated as

$$\Phi_{\text{eff}}(R) = \frac{1}{2} \sum_{i=1}^{2f} \langle \Phi_{\text{arm}}(\mathbf{u}_i; R) \rangle, \quad (5)$$

where the summation over all arms includes intra-star and inter-star interaction energies and $\langle \rangle$ denotes an ensemble average over configurations. Finally, the effective pair potential $v_{\text{eff}}(R)$ between the two stars is obtained as the change in the total energy of the system when the two stars are brought from infinite separation to separation R :

$$v_{\text{eff}}(R) = \Phi_{\text{eff}}(R) - \Phi_{\text{eff}}(\infty). \quad (6)$$

B. Torque Balance Analysis

As a check on our simulations, we also calculate the ground-state ($T = 0$) orientational distribution of arms, and the corresponding effective pair potential. At zero temperature, where Brownian motion is absent, mechanical equilibrium is reached when the net torque on each arm is zero. Electrostatic forces between arms generate torques that drive the arms to rotate against the friction of the solvent. Since the terminal angular velocity of an arm is proportional to the torque exerted on that arm, the equation of motion is²⁸

$$I_{\text{arm}} \frac{\partial \mathbf{u}_i}{\partial t} = -\gamma_{\text{arm}} \mathbf{u}_i \times \nabla_{\mathbf{u}_i} \Phi_{\text{arm}}(\mathbf{u}_i), \quad (7)$$

where I_{arm} and γ_{arm} are the arm's moment of inertia and rotational friction coefficient, respectively. The torque balance analysis amounts to finding the equilibrium configuration of the arms such that the right side of Eq. (7) vanishes.

In practice, we initialize the calculation by assigning random orientations to the arms and then use a simple forward-difference scheme to evolve the system until all of the arms stop rotating. This procedure efficiently generates the same final distribution as should be reached in a Monte Carlo simulation in which the only trial moves accepted are those that lower the energy. From the final arm distribution, we compute the ground-state effective pair

potential [from Eq. (6)], which represents a lower bound for the pair potential at nonzero temperature.

C. Density-Functional Theory

An alternative to modeling the arms explicitly is to consider an orientational distribution function (ODF) that describes the average configuration of the arms. We define the ODF $P(\mathbf{u}; \mathbf{r})$ such that $P(\mathbf{u}; \mathbf{r})d\mathbf{u}$ represents the average number of arms with orientation \mathbf{u} in a solid angle element $d\mathbf{u}$ subtended at the center of a star at position \mathbf{r} . The ODF is normalized to the number of arms: $\int d\mathbf{u}P(\mathbf{u}; \mathbf{r}) = f$. To approximate the ODF, we propose here a simple density-functional theory²⁹ based on a mean-field approximation.

In the case that translational and rotational time scales are sufficiently separated that center-of-mass and orientational coordinates decouple, the grand potential $\Omega[\rho(\mathbf{r}), P(\mathbf{u}; \mathbf{r})]$ is a functional of the single-star center-of-mass number density $\rho(\mathbf{r})$ and the arm ODF individually. An arbitrary external potential $\phi_{\text{ext}}(\mathbf{r})$ uniquely determines $\rho(\mathbf{r})$ and $P(\mathbf{u}; \mathbf{r})$, and thus the grand potential³⁰, which can be expressed as

$$\Omega[\rho(\mathbf{r}), P(\mathbf{u}; \mathbf{r})] = F_{\text{id}}[\rho(\mathbf{r}), P(\mathbf{u}; \mathbf{r})] + F_{\text{ex}}[\rho(\mathbf{r}), P(\mathbf{u}; \mathbf{r})] + \int d\mathbf{r} \int d\mathbf{u} \rho(\mathbf{r}) P(\mathbf{u}; \mathbf{r}) [\phi_{\text{ext}}(\mathbf{r}) - \mu], \quad (8)$$

where μ is the chemical potential of the arms and F_{id} and F_{ex} are the ideal-gas and excess Helmholtz free energy functionals, respectively. The ideal-gas free energy, associated with rotational entropy of the arms, is given exactly by

$$F_{\text{id}}[\rho(\mathbf{r}), P(\mathbf{u}; \mathbf{r})] = k_{\text{B}}T \int d\mathbf{r} \int d\mathbf{u} \rho(\mathbf{r}) P(\mathbf{u}; \mathbf{r}) [\ln(4\pi P(\mathbf{u}; \mathbf{r})) - 1], \quad (9)$$

translational entropy being ignored, assuming the star centers are fixed. The excess free energy, associated with interactions between arms, can be formally expressed as³⁰

$$\begin{aligned} F_{\text{ex}}[\rho(\mathbf{r}), P(\mathbf{u}; \mathbf{r})] &= \frac{1}{2} \int d\mathbf{r} \int d\mathbf{r}' \int d\mathbf{u} \int d\mathbf{u}' \int_0^1 d\lambda \rho^{(2)}(\mathbf{r}, \mathbf{r}'; [\lambda v_{\text{arm}}]) \\ &\times P^{(2)}(\mathbf{u}, \mathbf{u}'; \mathbf{r}, \mathbf{r}'; [\lambda v_{\text{arm}}]) v_{\text{arm}}(\mathbf{u}, \mathbf{u}'; \mathbf{r} - \mathbf{r}'), \end{aligned} \quad (10)$$

where $\rho^{(2)}(\mathbf{r}, \mathbf{r}'; [v_{\text{arm}}])$ is the two-star density, proportional to the probability of finding at

positions \mathbf{r} and \mathbf{r}' two stars whose arms interact via the pair potential $v_{\text{arm}}(\mathbf{u}, \mathbf{u}'; \mathbf{r} - \mathbf{r}')$ [Eq. (1)]; $P^{(2)}(\mathbf{u}, \mathbf{u}'; \mathbf{r}, \mathbf{r}'; [v_{\text{arm}}])$ is the two-arm orientational density, proportional to the probability of finding two arms at orientations \mathbf{u} and \mathbf{u}' on stars centered at \mathbf{r} and \mathbf{r}' ; and λ is a coupling constant that “turns on” the charge.

For two stars whose centers are fixed and separated by a displacement \mathbf{R} , the single-star density can be written as

$$\rho(\mathbf{r}) = \delta(\mathbf{r}) + \delta(\mathbf{r} - \mathbf{R}) \quad (11)$$

and the two-star density as

$$\rho^{(2)}(\mathbf{r}, \mathbf{r}'; [v_{\text{arm}}]) = \rho(\mathbf{r})\rho(\mathbf{r}'). \quad (12)$$

Combining Eqs. (8)-(12), and setting the external potential to zero, the grand potential simplifies to

$$\begin{aligned} \Omega[P(\mathbf{u})] = & 2 \int P(\mathbf{u}) \{k_{\text{B}}T[\ln(4\pi P(\mathbf{u})) - 1] - \mu\} \\ & + \int d\mathbf{u} \int d\mathbf{u}' \int_0^1 d\lambda \{P^{(2)}(\mathbf{u}, \mathbf{u}'; 0; [\lambda v_{\text{arm}}])v_{\text{arm}}(\mathbf{u}, \mathbf{u}'; 0) \\ & + P^{(2)}(\mathbf{u}, \mathbf{u}'; R; [\lambda v_{\text{arm}}])v_{\text{arm}}(\mathbf{u}, \mathbf{u}'; R)\}, \end{aligned} \quad (13)$$

where the factor of 2 in the first term accounts for the two stars and the dependence of $P(\mathbf{u})$ on R is now implicit. In general, the two-arm density can be written as

$$P^{(2)}(\mathbf{u}, \mathbf{u}'; R) = P(\mathbf{u})P(\mathbf{u}')g_{\text{arm}}(\mathbf{u}, \mathbf{u}'; R), \quad (14)$$

which simply defines the arm-arm pair distribution function $g_{\text{arm}}(\mathbf{u}, \mathbf{u}'; R)$, in such a way that, given an arm with orientation \mathbf{u} on a star centered at the origin, $P(\mathbf{u}')g_{\text{arm}}(\mathbf{u}, \mathbf{u}'; R)d\mathbf{u}'$ is the average number of arms with orientation \mathbf{u}' in solid angle $d\mathbf{u}'$ on a star centered at distance R .

To facilitate calculations, we make two approximations. First, we neglect arm-arm pair correlations and take $g_{\text{arm}}(\mathbf{u}, \mathbf{u}'; R) = 1$ for both inter- and intra-star arm-arm pair distribution functions. This mean-field approximation is based on the assumption that arm-arm interactions localize arms to the extent that correlations are mostly accounted for by the

anisotropic single-arm distribution function. Because this approximation neglects the self-correlation hole at $\mathbf{u} \simeq \mathbf{u}'$, it does give the wrong normalization for intra-star correlations, $\int d\mathbf{u} \int d\mathbf{u}' P^{(2)}(\mathbf{u}, \mathbf{u}'; 0) = f^2$, compared with the correct result $f(f-1)$. However, for multi-arm stars this is only a minor inconsistency. In passing, we note that our approximation for $g_{\text{arm}}(\mathbf{u}, \mathbf{u}'; R)$ is analogous to that commonly applied to the pair distribution function $g(\mathbf{r}, \mathbf{r}')$ of crystals, whose particles are localized to the extent that the structure of the two-particle density, $\rho^{(2)}(\mathbf{r}, \mathbf{r}') = \rho(\mathbf{r})\rho(\mathbf{r}')g(\mathbf{r}, \mathbf{r}')$, is dominated by that of the inhomogeneous one-particle density. As a second approximation, we assume that the arms of overlapping stars ($R < 2a$) do not interdigitate, but instead rotate backwards, being strictly excluded from a forward cone (Fig. 3), within which $P(\mathbf{u}) = 0$. The validity of the no-interdigitation approximation is examined below in Sec. IV.

With the above two approximations, Eq. (13) simplifies to

$$\begin{aligned} \Omega[P(\mathbf{u})] = & 2 \int d\mathbf{u} P(\mathbf{u}) \{k_{\text{B}}T[\ln(4\pi P(\mathbf{u})) - 1] - \mu\} \\ & + \int d\mathbf{u} \int d\mathbf{u}' P(\mathbf{u})P(\mathbf{u}') [v_{\text{arm}}(\mathbf{u}, \mathbf{u}'; 0) + v_{\text{arm}}(\mathbf{u}, \mathbf{u}'; R)]. \end{aligned} \quad (15)$$

At equilibrium, $\Omega[P(\mathbf{u})]$ is a minimum with respect to $P(\mathbf{u})$. Taking a functional derivative with respect to $P(\mathbf{u})$, we obtain

$$\frac{1}{2} \frac{\delta\Omega[P(\mathbf{u})]}{\delta P(\mathbf{u})} = k_{\text{B}}T \ln(4\pi P(\mathbf{u})) - \mu + \int d\mathbf{u}' P(\mathbf{u}') [v_{\text{arm}}(\mathbf{u}, \mathbf{u}'; 0) + v_{\text{arm}}(\mathbf{u}, \mathbf{u}'; R)]. \quad (16)$$

Setting the right side of Eq. (16) to zero yields an implicit equation for $P(\mathbf{u})$:

$$P(\mathbf{u}) = \frac{e^{\beta\mu}}{4\pi} \exp \left(-\beta \int d\mathbf{u}' P(\mathbf{u}') [v_{\text{arm}}(\mathbf{u}, \mathbf{u}'; 0) + v_{\text{arm}}(\mathbf{u}, \mathbf{u}'; R)] \right). \quad (17)$$

On the right side of Eq. (17), the first term of the integrand corresponds to interactions between arms in the same star (intra-star interactions) and the second term to interactions between arms in different stars (inter-star interactions). Note that, by symmetry, the two stars are mirror images of each other reflected in the perpendicular plane bisecting the line joining the star centers.

Once the equilibrium orientational distribution of arms is determined, the energy of the two-star system – a sum of the intra-star and inter-star arm interaction energies – can be

obtained from

$$\Phi_{\text{eff}}(R) = \int d\mathbf{u} \int d\mathbf{u}' P(\mathbf{u})P(\mathbf{u}') [v_{\text{arm}}(\mathbf{u}, \mathbf{u}'; 0) + v_{\text{arm}}(\mathbf{u}, \mathbf{u}'; R)], \quad (18)$$

which is the continuum analog of Eqs. (4) and (5) for the discrete model. The effective star-star pair interaction is finally calculated via Eq. (6), taking $P \rightarrow f/4\pi$ as $R \rightarrow \infty$.

IV. RESULTS AND DISCUSSION

Having described three methods for calculating the arm orientational distribution and the effective star-star pair potential, we now present and discuss numerical results. Our choice of parameters is restricted here by the defining criterion for weakly charged stars (Sec. II). In this parameter regime, where azimuthal arm-arm correlations are weak, we can exploit the axial symmetry of the ODF with respect to the line joining the centers of the two stars. Thus, the ODF is treated as a function of only the polar angle: $P(\mathbf{u}) = P(\theta)$. We have checked and confirmed this assumed symmetry in our MC simulations.

To extract $P(\theta)$ from the simulations, we bin the arm orientations in a manner illustrated in Fig. 4. Each sphere is partitioned into slices perpendicular to the line joining the star centers. Allowing each slice to subtend the same angle $\Delta\theta$, the average number of arms in the k^{th} slice centered at angle θ_k is $2\pi P(\theta_k) \sin \theta_k \Delta\theta$. The same number can also be expressed as $fN_k / \sum_{k=1}^M N_k$, where N_k is the number of occurrences (accepted trial moves) of an arm in the k^{th} slice and M is the total number of slices. Equating the two expressions,

$$P(\theta_k) = \frac{fN_k}{2\pi \sin \theta_k \Delta\theta \sum_{k=1}^M N_k}, \quad (19)$$

which is correctly normalized to the number of arms f .

To compute the corresponding DFT approximation for $P(\theta)$, we solve Eq. (17) iteratively, computing the arm-arm pair potentials $v_{\text{arm}}(\mathbf{u}, \mathbf{u}'; R)$ from Eq. (1). In practice, we construct a 60×60 grid on a sphere, with 60 equi-spaced longitudinal lines in the azimuthal coordinate ($0 < \phi < 2\pi$) and 60 equi-spaced latitudinal lines in the polar coordinate ($0 < \theta < \pi$). Starting from an initial normalized isotropic distribution, $P = f/4\pi$, we solve Eq. (17) self-consistently by numerical iteration until convergence. As a numerical check, we obtain the same results using Monte Carlo integration to compute the angular integral in Eq. (17) by

summing over randomly sampled directions.

Figure 5 compares our MC simulation results and DFT predictions for 8-arm stars, each of radius $a = 10$ nm and with 10 beads per arm, for a Debye screening constant $\kappa a = 1$ and various star valences and separations. The error bars represent root-mean-squared deviations from the average of intermediate averages over 100-cycle intervals. Evidently, the higher the valence and the closer the separation of the two stars, the more pronounced the anisotropy of the ODF, consistent with intuition. In the case of nonoverlapping stars, the DFT predictions agree well with simulation for a relatively low valence ($Z = 20$), as seen in Fig. 5(a). For a higher valence ($Z = 55$), the mean-field theory’s neglect of arm-arm correlations leads to an underestimation of the ODF structure [Fig. 5(b)].

In the case of overlapping stars, the DFT’s simplifying assumption of no interdigitation qualitatively models suppression of the ODF in the forward (small- θ) direction, but the sharp cut-off in $P(\theta)$ is clearly too severe. As Fig. 5(c) shows, Brownian motion at nonzero temperature can cause the forward arms of two overlapping stars to partially interdigitate. To quantify this behavior, we define an interdigitating configuration as one in which an arm on one star pierces a triangle whose vertices are the tips of two arms on the second star and the center of that star. Based on this criterion, we define the “interdigitation ratio” as the number of accepted configurations with interdigitating arms divided by the total number of accepted configurations. As Fig. 6 shows, the interdigitation ratio increases with decreasing star separation and with decreasing star valence. Nevertheless, the extent of interdigitation is sufficiently weak that the DFT’s neglect of such configurations still yields an accurate effective pair potential (see below).

To further quantify the extent of anisotropy in the arm orientational distribution, we define an orientational order parameter

$$S = -\langle \cos \theta \rangle = -\frac{2\pi}{f} \int_0^\pi d\theta \sin \theta \cos \theta P(\theta). \quad (20)$$

For a perfectly isotropic distribution, $S = 0$, whereas for a highly anisotropic distribution for which the ODF peaks at $\theta = \pi$, $S \cong 1$. Extracting the order parameter from a simulation

simply amounts to computing the sum

$$S = -\frac{1}{\sum_{k=1}^M N_k} \sum_{k=1}^M N_k \cos \theta_k. \quad (21)$$

Figure 7 displays the orientational order parameter as calculated from simulation for various choices of parameters, namely star valence, arm number, and screening length. As seen in Figs. 7(a) and (b), for fixed arm number the order parameter increases with increasing star valence and increasing screening length (decreasing screening constant). Figure 7(c) demonstrates that for fixed valence and screening length the order parameter increases upon reducing the number of arms (increasing charge per arm). Thus, orientational ordering (anisotropy) is amplified by strengthening or increasing the range of electrostatic interactions, which is consistent with the trends observed in the ODF (Fig. 5).

Interestingly, the degree of anisotropy does not vary monotonically with center-center distance between two stars. On the contrary, it attains a maximum at a distance where two stars strongly overlap, but short of complete overlap. The abrupt decrease in S at very short separations simply reflects the loss of identity of completely overlapping stars that merge into one isotropic “super-star.” As an aid to visualizing the anisotropy, Fig. 8 provides snapshots of the arm orientations of two 8-arm stars, as determined from the torque balance analysis and MC simulation.

Next, we compare results for the effective star-star pair potential, as computed from MC simulation, torque balance analysis, and DFT [Eqs. (5)-(7), (17), and (18)]. As seen in Fig. 9, the torque balance analysis predicts the lowest pair energy of the three methods, as expected of a method designed to find the ground state configuration. The actual energy is higher because of thermal rotational motion of the arms at nonzero temperature. The DFT predictions closely track the simulation data, aside from relatively small deviations at overlapping separations.

The consistent agreement between theory and simulation at all separations is somewhat unexpected, considering the significant discrepancies in arm orientational distributions for high valences and for overlapping stars [Fig. 5(c)]. The theory’s complete neglect of arm correlations and interdigitation is obviously unphysical for significantly overlapping stars, especially in the forward direction, *i.e.*, for small θ . As a consequence, the theory underestimates the density of (interdigitating) arms within the forward cone [Fig. 3] and overestimates

the arm density just outside of the forward cone. For stars that are only weakly overlapping, the ODF discrepancies are limited to arm configurations with small polar angles, which account for a relatively low fraction of the phase space in the angular integral for the effective pair potential [Eq. (18)]. For more strongly overlapping stars, the close agreement between theory and simulation must be attributed to a fortuitous cancellation of errors – namely an overestimate of the contribution to $v_{\text{eff}}(R)$ from arms outside of the interdigitation cone compensated by an underestimate of the contribution from interdigitating arms. Although it should be feasible to devise an analytical fit to our results for the effective pair potential of two overlapping stars for any set of system parameters, namely star radius, arm number, linear charge density, and screening length, we leave this fitting analysis to a future study.

For nonoverlapping stars, the simulation and DFT results hardly deviate from the predictions of linear response theory applied to an isotropic continuum model for the $1/r^2$ charge distribution of PE stars²⁰. The latter theory predicts a screened-Coulomb (Yukawa) potential between pairs of stars of the form

$$v_{\text{eff}}(R) = \frac{Z^2 e^2}{\epsilon} \left[\frac{\text{shi}(\kappa a)}{\kappa a} \right]^2 \frac{e^{-\kappa R}}{R}, \quad R > 2a, \quad (22)$$

where $\text{shi}(x) \equiv \int_0^x du \sinh(u)/u$ denotes the hyperbolic sine integral function. The accuracy of Eq. (22) may seem surprising, given the anisotropic arm distributions (Fig. 5). Closer examination reveals, however, that the anisotropy-induced reduction of inter-star interaction energy is largely balanced by an increase of the intra-star interaction energy, as illustrated in Fig. (10).

Finally, as a test of the validity of the rigid-arm-Yukawa model and the accuracy of our methods, we compare with results from molecular dynamics simulations of a molecular model of PE stars^{9,10} in which the arms are represented as bead-spring chains of Lennard-Jones particles connected by a finite-extension-nonlinear-elastic (FENE) potential and charged monomers and counterions interact via bare Coulomb potentials. The strong stretching of chains observed in the MD simulations^{9,10} allows direct comparison with our simpler rigid-arm model. To facilitate comparison, we choose parameters to match those given in Table IV of Jusufi *et al.*¹⁰, including the Debye screening length, Bjerrum length $e^2/\epsilon k_B T = 0.75$ nm, and fraction of charged beads per arm α . Following refs.^{9,10}, we treat the effective star valence Z as a tunable parameter to fit the effective pair force $F = -\partial v_{\text{eff}}(R)/\partial R$. (Note that

tuning Z also changes the screening length.) From the effective valence, we then obtain the effective number of counterions condensed inside the two stars, $N_1 = 2(fN_b\alpha - Z)$. As shown in Fig. 11, our best fits to the MD forces between overlapping pairs of stars with charging fraction $\alpha = 1/4$ are obtained by choosing $N_1 = 137$ for 10-arm stars and $N_1 = 465$ for 30-arm stars. For comparison, the corresponding MD values³¹ are, respectively, $N_1 = 147$ and $N_1 = 450$. The excellent fit of the MC and MD force data, in particular the close agreement of the effective number of condensed counterions, provides a consistency check and supports the simple rigid-arm-Yukawa model for the weakly charged stars considered here. Further such comparisons would be useful to establish the limits of validity of the model.

Three issues merit further discussion. First, while molecular models that include chain flexibility and explicit microions naturally provide the most realistic description of PE stars, the many degrees of freedom present major computational challenges. Simulations of such models have thus far been limited to only one or two stars^{8,9,10}. By comparison, the relatively coarse-grained model explored here seems to accurately capture effective interactions between PE stars, yet is simple enough to allow studies of phase behavior in simulations of many interacting stars.

Second, although simulations of the coarse-grained and molecular models yield very similar pair forces, the rather different treatments of the microions in the two models suggest complementary physical interpretations. In the molecular model, the interactions between overlapping stars are attributed largely to entropy of trapped counterions, electrostatics playing only a relatively minor role^{9,10}. In contrast, in the coarse-grained one-component model, where the microions are integrated out in a first step to obtain effective (screened-Coulomb) arm-arm interactions, electrostatics is the sole determiner of effective star-star interactions. Thus, the entropy of trapped counterions, which in the molecular model is explicitly associated with the distribution of counterions around the arms of the stars, has its coarse-grained counterpart in the implicit contribution of counterions to the effective star valence and to the effective interactions via the Debye screening constant. Although the correspondence between the two models has been tested here using the available MD data for 10-arm and 30-arm stars [Fig. 11], it should be tested more extensively in future, especially over a broader range of star functionality.

Third, the PE stars considered here belong to a class of macromolecules for which chain entropy is negligible. Since we model the arms as charged rigid rods, and ignore excluded-

volume interactions between arms, the effective pair interactions vanish in the limit of charge-neutral stars. For stars with flexible arms, Witten and Pincus³² and Likos *et al.*³³ have shown that conformational entropy of the arms generates an effective “ultrasoft” repulsion between neutral stars, which varies logarithmically with distance at small separations and follows a Yukawa form at longer separations. Such entropic interactions are here neglected.

V. SUMMARY AND CONCLUSIONS

In summary, within a coarse-grained model of polyelectrolyte stars, we have analyzed arm orientational anisotropy and effective interactions between an isolated pair of weakly charged (orientationally molten) stars. The arms of the stars were modeled as rigid rods, freely rotating about the star centers, and carrying evenly spaced charged beads. Microions were included implicitly by modeling electrostatic interactions between pairs of charged beads via an effective screened-Coulomb (Yukawa) potential. Arm orientational distribution functions and effective star-star electrostatic interactions were calculated by three independent methods: Monte Carlo simulation, torque balance analysis, and density-functional theory.

The arm orientational distributions predicted by DFT are in good agreement with simulation for nonoverlapping stars of relatively low effective valence. With increasing overlap and increasing valence, the agreement worsens due to the theory’s neglect of arm-arm correlations and interdigitation. An orientational order parameter, quantifying the extent of anisotropy, increases as two stars approach each other, peaks at strong overlap, and then decreases as the stars near complete overlap.

The simulation and DFT results for the effective pair potential between nonoverlapping stars are in excellent agreement with previous predictions of linear response theory applied to a continuum model of PE stars with isotropic $1/r^2$ charge distribution²⁰. This close agreement results not only from the relatively weak anisotropy of separated stars, but also from a fortuitous cancellation between reduced inter-star interactions and enhanced intra-star interactions induced by arm anisotropy. We conclude that electrostatic interactions between nonoverlapping weakly charged PE stars can be accurately modeled by a simple Yukawa effective pair potential.

The effective pair potentials from our Monte Carlo simulations and DFT calculations are in good agreement over the whole range of star separations, including strongly overlapping

stars, for the parameters here investigated. Furthermore, treating the effective valence of the stars as a fitting parameter, we achieve a close fit to available data for the effective pair forces and numbers of condensed counterions from MD simulations^{9,10} of a molecular model with flexible bead-spring chains and explicit counterions.

Simulations of many-star systems are a natural next step. For dilute solutions, interactions between isolated pairs of nonoverlapping stars can be reliably approximated, as confirmed here, by an isotropic screened-Coulomb pair potential²⁰. Only interactions between overlapping stars must then be computed by explicit summation over pairs of charged beads, pending an analytical fit to our MC data. For concentrated solutions of frequently overlapping stars, arm anisotropy and many-body interactions among three or more stars are likely to be important. In this regime, explicit pairwise summation over beads is essential. Such an approach could independently test the phase behavior predicted by recent simulations of dense solutions of stars interacting via isotropic effective pair potentials³⁴.

Acknowledgments

We thank Ben Lu, Shrikant Shenoy, and Christos N. Likos for helpful discussions. This work was supported by the National Science Foundation under Grant No. DMR-0204020.

-
- ¹ F. Oosawa, *Polyelectrolytes* (Dekker, New York, 1971); *Polyelectrolytes*, ed. M. Hara (Dekker, New York, 1993).
 - ² G. M. Gratson, M. Xu, and J. A. Lewis, *Nature* **428**, 386 (2004).
 - ³ Y. Kakizawa and K. Kataoka, *Adv. Drug Deliv. Rev.* **54**, 203 (2002).
 - ⁴ K. C. Wood, J. Q. Boedicker, D. M. Lynn, and P. T. Hammond, *Langmuir* **21**, 1603 (2005).
 - ⁵ C. N. Likos, *Phys. Rep.* **348**, 267 (2001).
 - ⁶ P. Pincus, *Macromol.* **24**, 2912 (1991).
 - ⁷ J. Klein Wolterink, J. van Male, M. Daoud, and O. V. Borisov, *Macromol.* **36**, 6624 (2003).
 - ⁸ M. Roger, P. Guenoun, F. Muller, L. Belloni, and M. Delsanti, *Eur. Phys. J. E* **9**, 313 (2004).
 - ⁹ A. Jusufi, C. N. Likos, and H. Löwen, *Phys. Rev. Lett.* **88**, 018301 (2002).
 - ¹⁰ A. Jusufi, C. N. Likos, and H. Löwen, *J. Chem. Phys.* **116**, 11011 (2002).
 - ¹¹ Y. Mir, P. Auroy, and L. Auvray, *Phys. Rev. Lett.* **75**, 2863 (1995).

- ¹² P. Guenoun, F. Muller, M. Delsanti, L. Auvray, Y. J. Chen, J. W. Mays, and M. Tirrell, *Phys. Rev. Lett.* **81**, 3872 (1998).
- ¹³ W. Groenewegen, S. U. Egelhaaf, A. Lapp, and J. R. C. van der Maarel, *Macromol.* **33**, 3283 (2000).
- ¹⁴ X. Guo and M. Ballauff, *Phys. Rev. E* **64**, 051406 (2001).
- ¹⁵ W. Groenewegen, A. Lapp, S. U. Egelhaaf, and J. R. C. van der Maarel, *Macromol.* **33**, 4080 (2000).
- ¹⁶ V. M. Prabhu, E. J. Amis, D. P. Bossev, and N. Rosov, *J. Chem. Phys.* **121**, 4421 (2004).
- ¹⁷ V. M. Prabhu, B. D. Vogt, W. Wu, J. F. Douglas, E. K. Lin, S. K. Satija, D. L. Goldfarb, and H. Ito, *Langmuir* **21**, 6647 (2005).
- ¹⁸ B. Das, X. Guo, and M. Ballauff, *Prog. Colloid Polym. Sci.* **121**, 34 (2002).
- ¹⁹ O. V. Borisov, T. M. Birshtein, and E. B. Zhulina, *J. Phys. II* **1**, 521 (1991).
- ²⁰ A. R. Denton, *Phys. Rev. E* **67**, 011804 (2003).
- ²¹ H. Wang and A. R. Denton, *Phys. Rev. E* **70**, 041404 (2004).
- ²² Y. Wang *et al.*, *Biochemistry* **30**, 5667 (1991).
- ²³ X. Wang, W. H. Daly, and P. Russo, *Biomacromolecules* **2**, 1214 (2001).
- ²⁴ D. M. Heuer, S. Saha, and L. A. Archer, *Biopolymer* **70**, 471 (2003).
- ²⁵ G. Brodowski, A. Horvath, M. Ballauff, and M. Rehahn, *Macromol.* **29**, 6962 (1996).
- ²⁶ H. Wang and A. R. Denton (in preparation).
- ²⁷ D. Frenkel and B. Smit, *Understanding Molecular Simulation* (Academic Press, 1996).
- ²⁸ M. Doi and S. F. Edwards, *The Theory of Polymer Dynamics* (Oxford University Press, New York, 1986).
- ²⁹ D. W. Oxtoby, in *Liquids, Freezing and Glass Transition*, Les Houches session 51, edited by J.-P. Hansen, D. Levesque, and J. Zinn-Justin (Elsevier, New York, 1990).
- ³⁰ R. Evans, *Adv. Phys.* **28**, 143 (1979).
- ³¹ Due to a typographical error in Table IV of Jusufi *et al.*¹⁰, the value of N_1 given for $f = 30$ arms should be 450 (not 265) (C. N. Likos, private communication).
- ³² T. A. Witten and P. A. Pincus, *Macromol.* **19**, 2509 (1986).
- ³³ C. N. Likos, H. Löwen, M. Watzlawek, B. Abbas, O. Jucknischke, J. Allgaier, and D. Richter, *Phys. Rev. Lett.* **80**, 4450 (1998).
- ³⁴ N. Hoffmann, C. N. Likos, and H. Löwen, *J. Chem. Phys.* **121**, 7009 (2004).

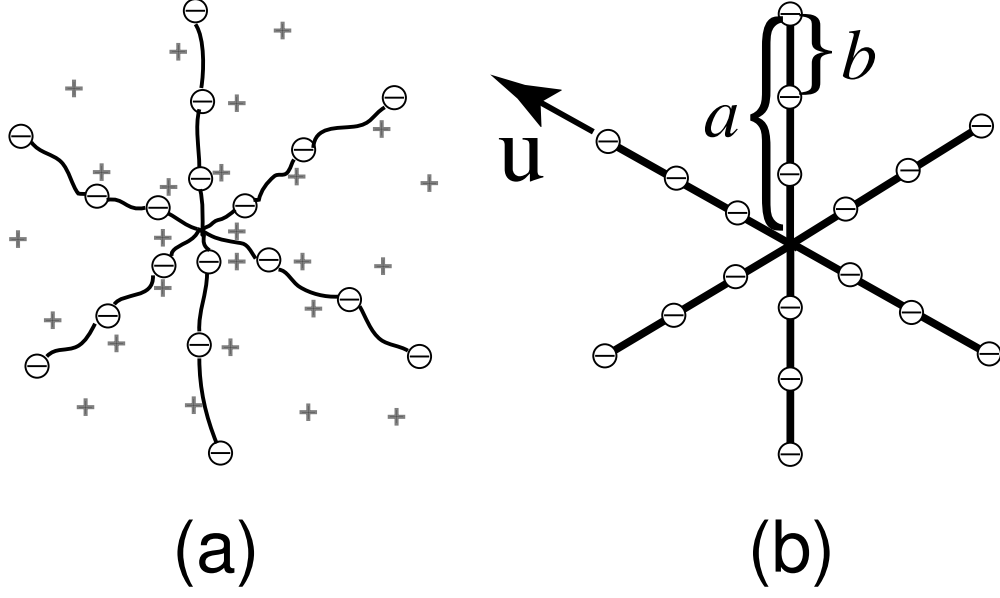


FIG. 1: (a) Schematic drawing of PE star and counterions. (b) Model of PE star with rigid, rodlike arms. Integrating out degrees of freedom of the microions leads to an effective Yukawa pair potential between pairs of charged beads along the arms.

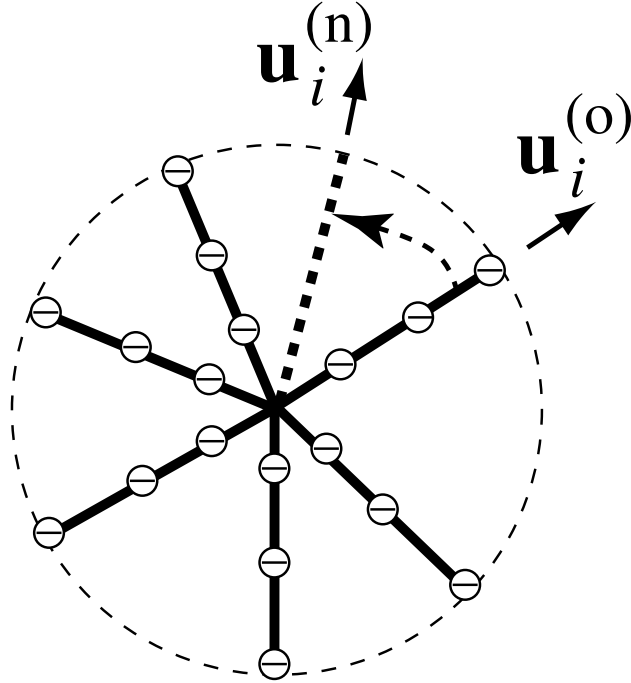


FIG. 2: Trial rotation of the i^{th} arm from its old orientation $\mathbf{u}_i^{(o)}$ to its new orientation $\mathbf{u}_i^{(n)}$.

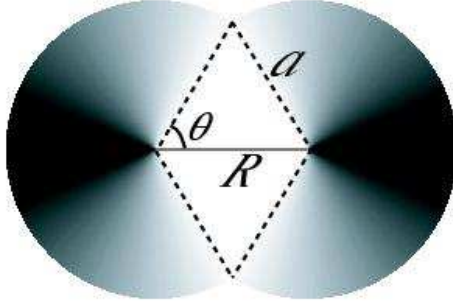


FIG. 3: Geometry assumed in density-functional theory of overlapping stars. Arms are completely excluded from cone-shaped volumes (white region). Darker shading indicates higher arm density.

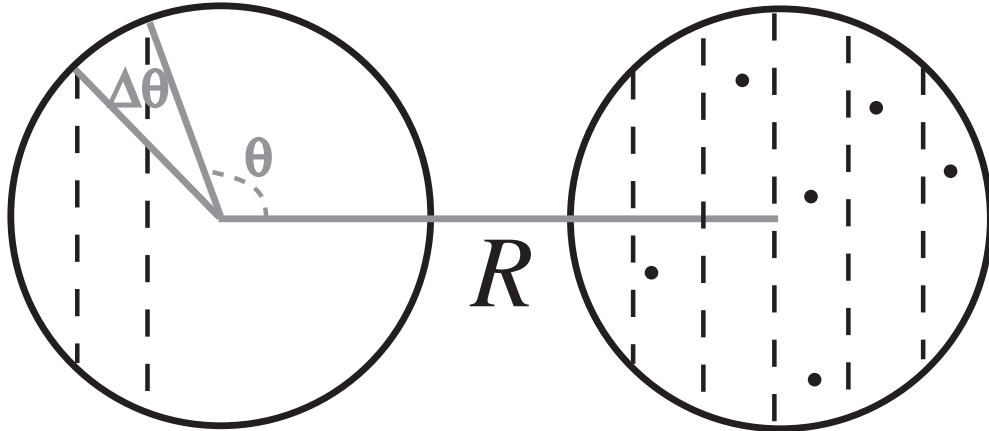


FIG. 4: Illustration of Monte Carlo data analysis. Dashed lines represent slices of spheres perpendicular to center-center line between stars. Points indicate positions of arm tips at various polar angles θ , each slice subtending an angle $\Delta\theta$. Statistical analysis of configurations yields the arm orientational distribution function.

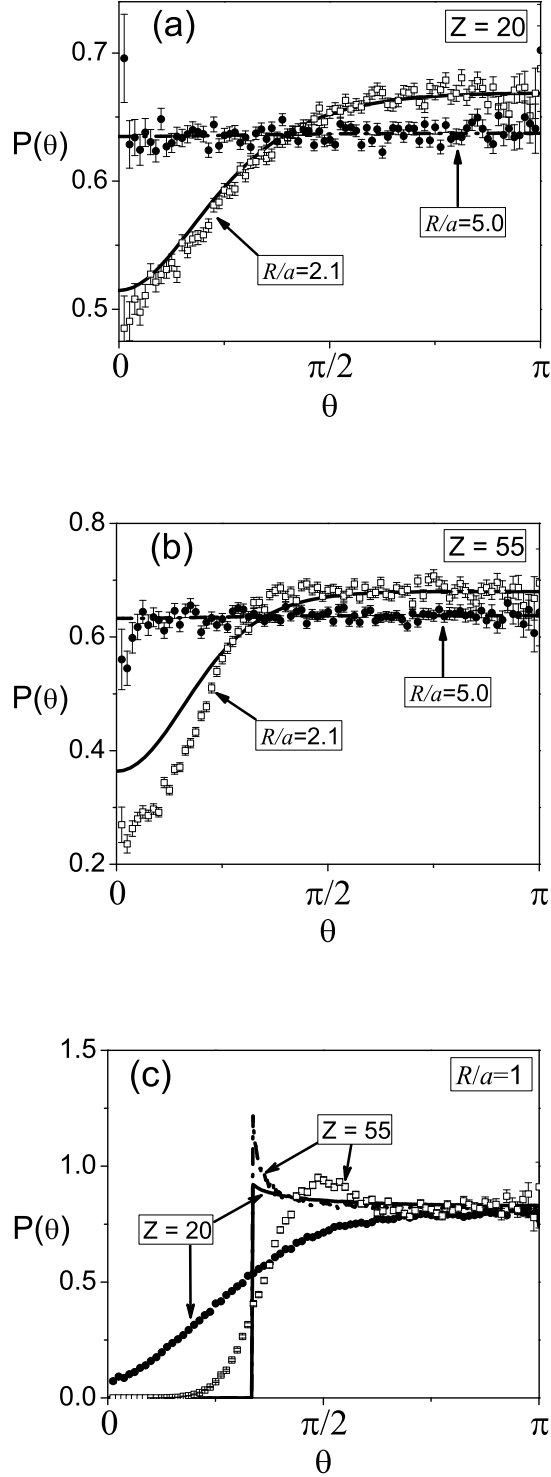


FIG. 5: Arm orientational distribution function $P(\theta)$ vs. polar angle θ for two 8-arm stars of radius (arm length) $a = 10$ nm, with 10 beads per arm, Debye screening constant $\kappa a = 1$, and various labeled star valences Z and center-center separations R . Results from Monte Carlo simulation (symbols) and density-functional theory (curves) are compared. Error bars represent statistical uncertainty (one standard deviation) in simulation data.

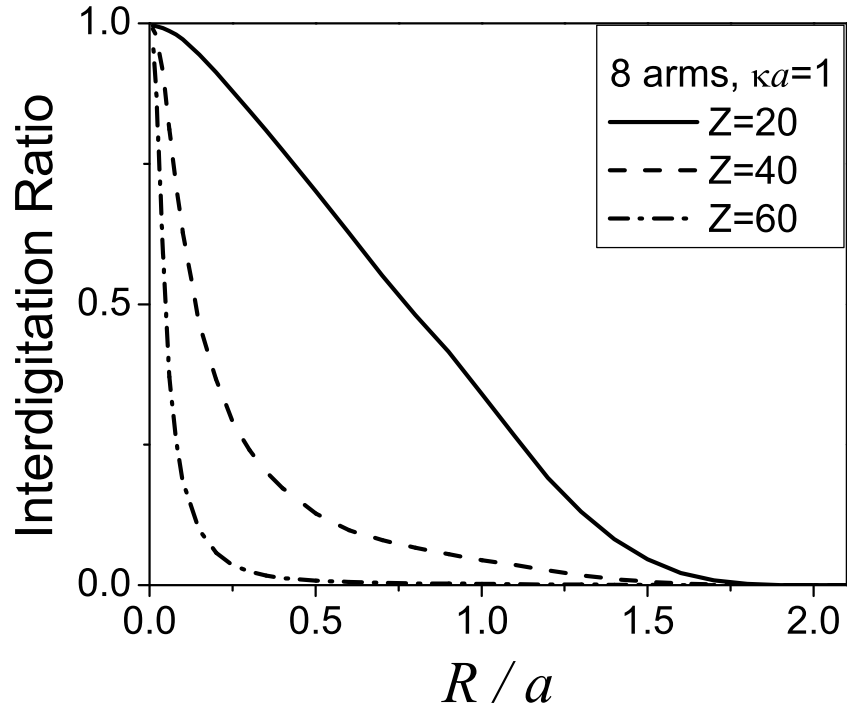


FIG. 6: Fraction of interdigitating configurations (see text) for two overlapping 8-arm stars of various valences at fixed screening constant $\kappa a = 1$.

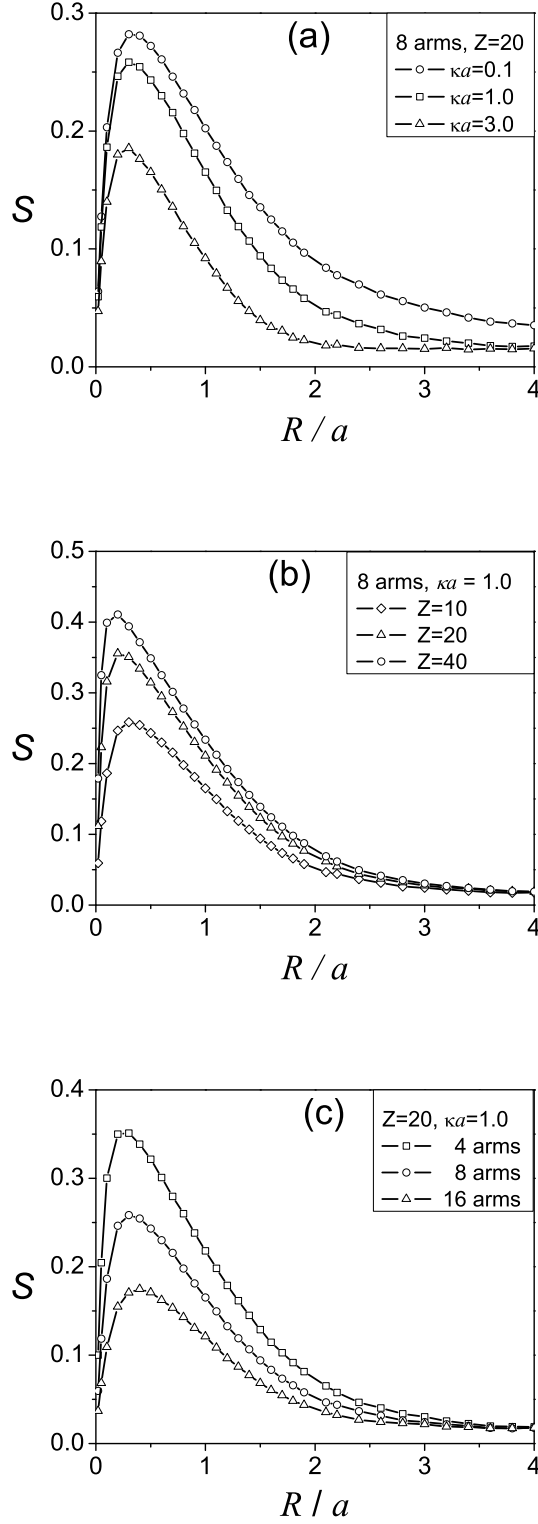


FIG. 7: Orientational order parameter S vs. center-center separation R between two stars of radius $a = 10$ nm, with 10 beads per arm, for various parameter combinations. (a) Fixed arm number and star valence, varying screening length. (b) Fixed arm number and screening length, varying star valence. (c) Fixed screening length and valence, varying arm number. Symbols are simulation data and curves are guides to the eye.



FIG. 8: Configurations of two approaching stars at center-center distance $R/a = 1$ (upper panel) and $R/a = 0.2$ (lower panel) from a torque balance analysis. Each star has 8 arms of length 10 nm, with 10 beads per arm, valence $Z = 20$, and screening constant $\kappa a = 1$.

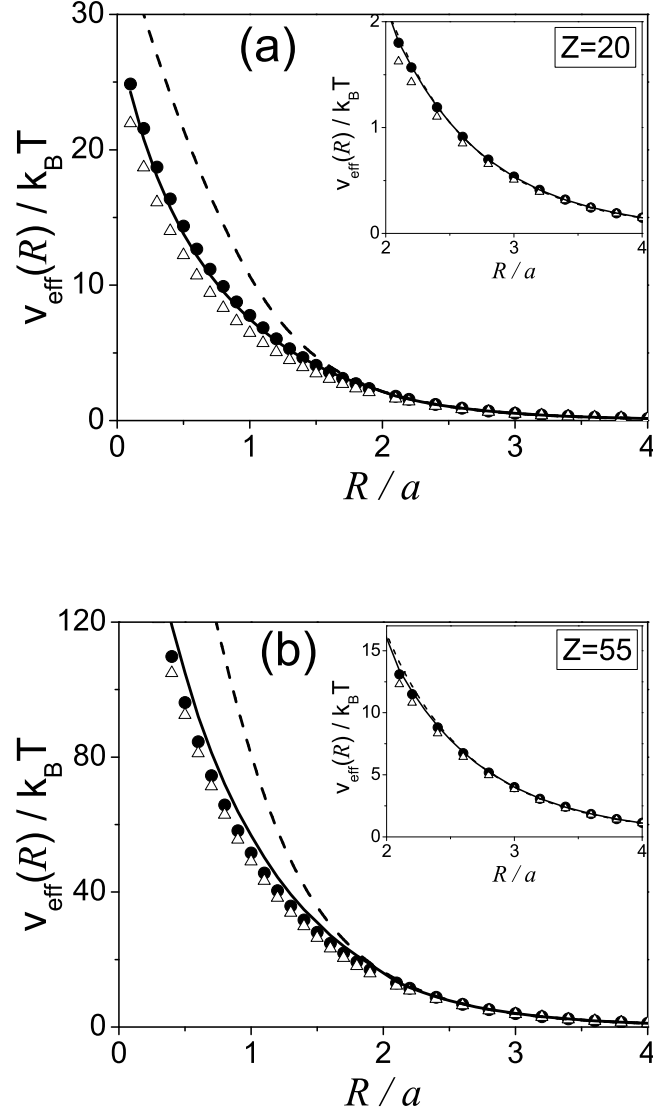


FIG. 9: Effective pair potential vs. center-center separation between an isolated pair of 8-arm stars of valence (a) $Z = 20$ and (b) $Z = 55$, calculated from Monte Carlo simulation (\bullet), density-functional theory (solid line), torque balance analysis (\triangle), and linear response theory+continuum model²⁰ (dashed line). Insets magnify nonoverlapping region.

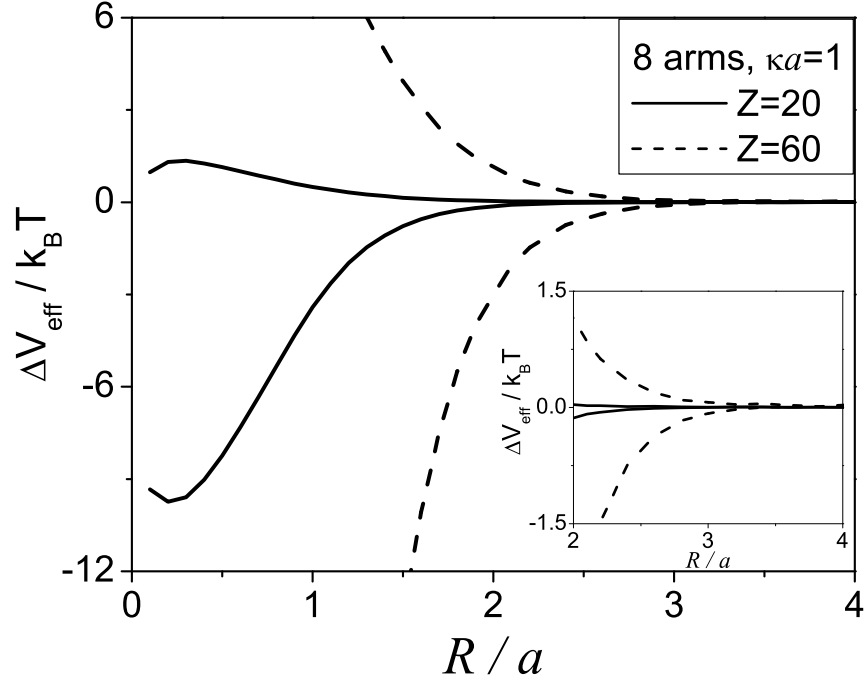


FIG. 10: Monte Carlo simulation results for anisotropy-induced changes in inter- and intra-star pair interaction energies for 8-arm stars with arm length $a = 10$ nm, 10 beads per arm, and screening constant $\kappa a = 1$. Solid and dashed curves are intra-star (upper) and inter-star (lower) energies for star valences $Z = 20$ and $Z = 60$, respectively. Inset magnifies nonoverlapping region.

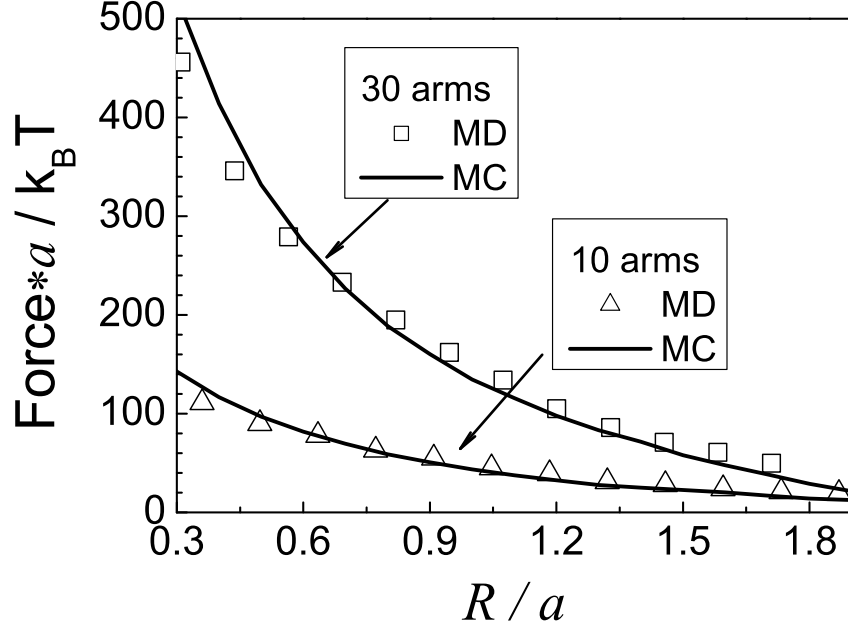


FIG. 11: Comparison of forces between two stars of radius a vs. center-center separation R from our Monte Carlo (MC) simulations of the rigid-arm-Yukawa model (curves) and molecular dynamics (MD) simulations of a molecular model (symbols)¹⁰. Choosing the number of condensed counterions as $N_1 = 137$ for 10-arm stars and $N_1 = 465$ for 30-arm stars yields good agreement between MC and MD data (see text).